# Fiber-Optic Subcarrier Multiplexed CDMA Local-Area Networks for Subband Image Transmission

Po-Rong Chang, *Member, IEEE*, and Chih-Chiang Chang

*Abstract*—**This paper investigates the application of subcarrier multiplexed code-division multiple-access (CDMA) techniques to image transmission over fiber-optic local-area networks (LAN's). In the hybrid scheme, CDMA is used to suppress the interference caused by the laser nonlinearity in the subcarrier multiplexing (SCM) fiber-optic communication systems. Likewise, the SCM scheme is able to increase the channel data rate of CDMA systems. This hybrid system combines the advantages of both schemes and is particularly well suited to subband coding that divides the image information into multiple parallel data streams using an analysis filter bank, each of which is transmitted via a unique subcarrier-code pair, where the spreading code and subcarrier frequency correspond to the image and one of its subbands, respectively. This hybrid scheme also allows more than one image to be transmitted and be accessed simultaneously at the same channel bandwidth, in which each image is assigned a particular spreading code added to its digital data modulating the subcarrier. After transmission, each received signal is independently recovered at a high-Q surface acoustic wave (SAW) receiver with the matching subcarrier-code pair. Other concurrent signals are rejected by the SAW. Then, all the recovered subbands are reassembled by a synthesis filter bank into a close reproduction to the original image. In this paper, the image quality of subband image transmission via CDMA/SCM fiber-optic channels is evaluated and examined.**

## I. Introduction

TRANSMISSION of broad-band video over fiber-optic networks has been carried out primarily using microwave subcarrier multiplexing (SCM) followed by laser modulation [1]. Because of its flexibility and cost-effectiveness, SCM technology can also be used as a basic building block in advanced lightwave systems, such as wavelength-division multiplexing (WDM) systems, in which the digital data of each video channel are assigned to a specific and separate wavelength. The system requires accurate wavelength control of all lasers, and tunable narrow-band optical fibers at the receiver. For SCM systems, the entire subcarrier video band is intensity modulated onto the light source, producing a single analog light wave containing the multiplexed video channels. The fiber then distributes the light via a star network. Since the laser light source is modulated by a combination of total video bands, the system suffers from two basic limitations: 1) the interference due to harmonics and intermodulation products (IMP's) caused by the nonlinearities of the laser modulation characteristics and 2) the inherent power robbing due to the sum of many signals simultaneously modulating over a limited laser dynamic range. The performance of each individual channel video will severely deteriorate as the number of subcarriers increases because the amplitude of a total of IMP's and harmonics noise increases with the number of video channels or subcarriers. Likewise, the power robbing forces the power levels of each individual subcarrier to be scaled inversely proportional to the number of subcarriers in order to maintain the total loading level on the laser. This implies that the individual channel video performance is further reduced as more simultaneous subcarriers are added to the system.

An alternative method for digital video multiplexing is code-division multiple-access (CDMA), in which data of a video source are coded into addressed lightwave pulse sequence that can be recognized and separated at the receiver. Gagliardi *et al.* [3] and Kitayama [4] proposed the all-optical implementations of the CDMA systems which are applied to image transmission over a fiber optic network, where tunable lasers with accurate wavelength control are not required. This technique can also be used for suppressing the effect of interference due to harmonics and IMP's caused by laser nonlinearity in the subcarrier multiplexing schemes. However, a prime disadvantage with CDMA is the sacrifice in channel data bit rate (relative to speeds available in the laser itself) that occurs in the insertion of code addressing [27]. For typical laser sources, this generally limits the channel data bit rates to tens of megahertz. Hence, optical CDMA for the video transmission application will be competitive only when individual channel video bit rates can be significantly reduced.

To attain the higher channel data bit rate and maximum image quality, a hybrid scheme that combines SCM and CDMA is used, where a splitting process is required to divide the image information into a large number of independent data streams, each of which is transmitted using one of subcarrier frequencies, and can fit the narrow-band data rate requirement of SCM schemes [5]. The hybrid CDMA/SCM scheme allows more than one image to be transmitted and be accessed simultaneously at the same channel bandwidth, in which each image is assigned a particular spreading code sequence added to its digital data modulating a carrier. Khaleghi and Kavehrad [6] showed that the resulting hybrid CDMA/SCM system is

Manuscript received May 1, 1995; revised September 9, 1995. This work was supported in part by the National Science Council of Taiwan, R.O.C., under Contract NSC85-2221-E009-034.

The authors are with the Department of Communication Engineering, National Chiao-Tung University, Hsin-Chu, Taiwan, R.O.C. (email: prchang@cc.nctu.edu.tw; u8111844@cc.nctu.edu.tw).

Publisher Item Identifier S 0733-8716(96)05233-X.

robust against interference and is more spectrally efficient than a CDMA system.

In this paper, an image splitting process adopted here is based on subband coding which is one of the less complex encoding algorithms [7]–[9]. The principle of subband coding is based on the decomposition of the input image into a number of narrow bands using analysis filter bank where each band is then decimated, coded and assigned to a unique pair of spreading code and subcarrier frequency separately. The spreading code and subcarrier frequency correspond to the image and one of its subbands, respectively. In addition to achieving the highest possible image quality and maximum spectrum utilization, the input image should be decomposed into a sufficient number of subbands where each band is spread to full channel bandwidth. After transmission, each signal sample is then independently recovered at a surface acoustic wave (SAW) receiver with a very high-Q and a unique preprogrammed code sequence. Each SAW only responds to the desired subband tuned to its center subcarrier frequency and with the matching code. Other concurrent subbands are rejected by the SAW. These recovered subbands are reassembled by the synthesis filter bank into a close approximation to the input image. For dividing the image into subbands, the symmetric short kernel filters [9], [10], [25] (SSKF's) are used for filtering. These filters require a very small number of coefficients and are necessary to keep the implementation complexity at a low level. In Section IV, we will discuss the transmission error effects in the subband image via the hybrid CDMA/SCM fiber-optic channels [5], [6]. Bit errors in an individual subband will generate error contributions at the receiver output within that frequency band. Since the channel error contributions in different subbands are expected to be uncorrelated, the total channel error variance in the recovered image equals the sum of these errors. Moreover, we will show that the total channel error variance is in proportion to the bit-error rate (BER) when the BER is sufficiently small. This would lead to the image signal-to-noise ratio (SNR) being inversely related to a logarithmic function of the bit error rate. Section IV shows computer simulations used to evaluate the image SNR performance of subband image transmission by hybrid CDMA/SCM systems.

## II. Transmission of Subband-Coded Images Over Fiber-Optic Subcarrier Multiplexed CDMA Networks

In the multiple-access system for image transmission of interest, the system is assumed to multiplex a set of digital video signals by utilizing a combination of CDMA and SCM schemes. The system block diagram is depicted in Fig. 1. At the inputs to the system, signals from a cluster of data terminals share the same laser light source. Each cluster is uniquely defined by a sequence of chips, $a_k$. Every transmit terminal has a tunable oscillator capable of generating several discrete FDM subcarrier frequencies, i.e., $f_1, f_2, \cdots, f_M$, ranging from 45 to 700 MHz. The $j$th FDM subcarrier frequency would be assigned to the $j$th data terminal belonging to each cluster. The sequence of chips is added to the information bits and then spreads the narrow band of data. The tunable oscillator FDM subcarrier signal is modulated by the spread data. Sum of the FDM signals intensity modulates a light source. Emitted light is guided to a passive star coupler which can distribute signals among a number of output ports connected to the LAN users via an optical fiber. The signals from the users in the same or different clusters are mutually protected by the difference in either the subcarrier frequency or spreading code. On the receiver side, each user has a SAW matched-filter with a very high-Q and a unique preprogrammable code sequence. Similarly, SAW filters belonging to a cluster of users share the same photodetector. Each SAW only responds to the desired signal tuned to its center subcarrier frequency and with the matching spreading code. Other concurrent signals are rejected by the SAW. In other words, the data from the $k$th user (terminal) in the $j$th cluster can be recovered by the SAW receiver with a pair $a_j$ and $f_k$. Practically there will be no interference between the shared bands when the subcarrier frequencies are spaced by one narrow-band data rate. For example, Khaleghi and Kavehrad [5] showed that the subcarriers at 120, 120.08, 120.16 MHz, etc. create no significant interference for one another even if they all carry the same spreading code sequence in the same cluster at a data rate of 80 kb/s when they are spaced by 80 kHz. However, the required double-sided subcarrier modulation band is 20 MHz for the spread signal at a chip rate of 10 Mchips/s and can be reused by the subcarrier, as long as they are 80 kHz apart. This is because a SAW filter has a sinc function amplitude response with nulls on each side of the main lobe by one data rate away from the center frequency.

Clearly from Fig. 2, it may be found that the hybrid CDMA/SCM scheme is particularly well suited to subband coded image transmission, where each image and its subband correspond to a specific cluster (spreading code) and a user (subcarrier frequency) belonging to the cluster respectively. In other words, the $k$th subband of the $j$th image is transmitted via the $k$th subcarrier frequency, $f_k$, and the $j$th spreading code, $a_j$. As shown in Fig. 2, each field in a video sequence is decomposed into several components (four in the Fig. 2) using a bank of filters (i.e., $H_{ll}(z_1, z_2)$, $H_{lh}(z_1, z_2)$, $H_{hl}(z_1, z_2)$, $H_{hh}(z_1, z_2)$) called the analysis filter bank. The lowest frequency component is a lower resolution version of the original scene, and the high frequency components mostly carry information about the contours, edges and other finer details. These filtered signals are then downsampled to yield the subband signals. The downsampling following the analysis filter bank reduces the sampling rate of each of the $M$ subband signals to $\frac{1}{M}$ times the input signal sampling rate. As a result, these filters decompose the signal into $M$ equally spaced subbands at the same time. For example, if the Quarter Common Intermediate Format (QCIF) CCITT standard videophone image of 180 pels by 144 lines is at 29.97 frames/s, it yields about 64 kb/s [2]. For $M = 4$, the bit rate of each subband can be reduced to 16 kb/s. For the next generation personal communication networks (PCN's), the broadband integrated services digital network (B-ISDN), based on lightwave technology, is expected to become the preeminent multimedia broadband network for a wide variety of digital video services such as video-on-demand

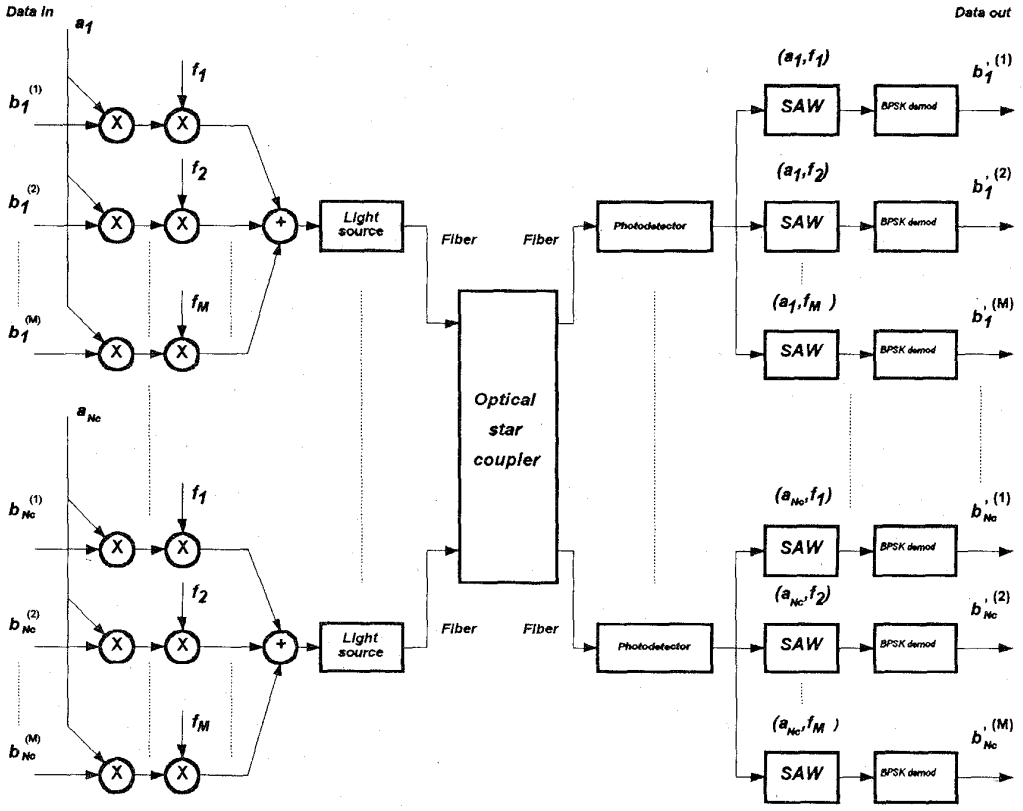


Fig. 1. LAN configuration for a fiber-optic subcarrier multiplexed CDMA system, where $N_c$ is the number of clusters (spreading codes), $M$ is the number of users in each cluster, $a_1, a_2, \cdots, a_{N_c}$ are the spreading codes, and $f_1, f_2, \cdots, f_M$ are the sinusoidal subcarriers.

(VOD), HDTV, MPEG and interactive video/multimedia applications. The ITU-TS has adopted a unversal network node interface (NNI) with a standard bit rate of 155.5 Mb/s $\times n$ ($n$: integer) as the first-step toward realizing a truly effective B-ISDN. It is possible to use the hybrid CDMA/SCM scheme to support such high bit rate video services by increasing the number of decomposed subbands. With a sufficient number of subbands or streams, each subband can fit within the narrowband data rate requirement. In other words, an image of rate $Mr_b$ is disassembled (demultiplexed) into $M$ subsequences each of rate $r_b$. Each subsequence is transmitted using one of $M$ subcarrier frequencies and a specific spreading code associated with the image. For $N_c$ images, there are $MN_c$ subsequences which can be transmitted at the same time over the optical channel. Each received subsequence is independently recovered at the SAW match filter with its own subcarrier frequency and spreading code pair. At the receiver, the $M$ recovered subsequences or subbands are then decoded, upsampled, and reassembled (multiplexed) by the synthesis filter bank into a close approximation to the input scene.

In this paper, the focus is on intra-field subband coding and the exploitation of temporal correlation that can be carried out by a three-dimensional (3-D) subband system [11] which consists of temporal, horizontal, and vertical filterings. Undoubtedly, the hybrid CDMA/SCM system can be applied to the subband system directly. However, the use of intra-field coding is motivated by the goal to keep the decoder cost low. The implementation is relatively simple since frame stores and motion detection/estimation hardware is not required. Each field in the video sequence is represented by using two-dimensional (2-D) subband coding [15].

### A. Hybrid CDMA/SCM Model

The hybrid CDMA/SCM technique is able to achieve the high transmission bit-rate services of more than one image via the optical channel. For $N_c$ images transmitted at $N_c$ different locations (or clusters), each of them is divided into $M$ subband images which have their own subcarrier frequencies. During each $T$ second symbol interval, the $j$th transmitting laser is amplitude-modulated by the sum of modulated signals of different $M$ subbands in the image (cluster), and the modulated signal for each subband is the product of data which takes on values $\{-1, 1\}$, a spreading code sequence, and a sinusoidal subcarrier. The modulated signal for the $k$th subband (user) of the $j$th image is expressed as

$$s_{kj}(t) = Aa_j(t)b_j^{(k)}(t)\cos(2\pi f_k t + \phi_{kj}) \tag{1}$$

where $a_j(t)$ denotes the spreading code corresponding to the $j$th image, $b_j^{(k)}$ represents a data signal for the $k$th subband of the $j$th image, respectively, $A$ is the signal amplitude, $f_k$ denotes the $k$th subcarrier frequency, and $\phi_{kj}$ is a random carrier phase, uniformly distributed between zero and $2\pi$.

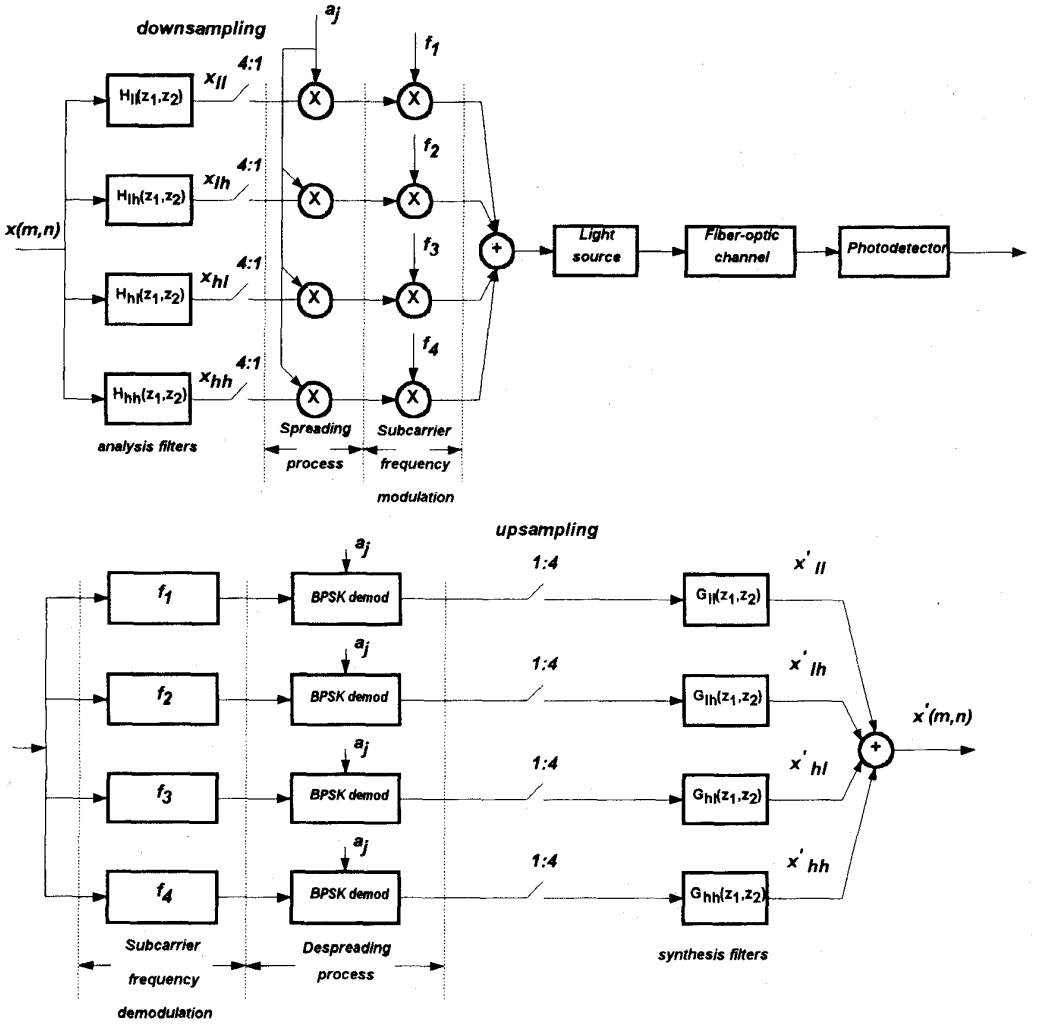


Fig. 2. Transmission of subbands for the $j$th image via fiber-optic CDMA/SCM channel, where $a_j$ is the spreading code, $f_k$ is the subcarrier frequency, $1 \leq j \leq N_c$. $1 \leq k \leq M$, and $M = 4$.

$b_j^{(k)}(t)$ and $a_j(t)$ are defined as follows:

$$b_j^{(k)}(t) = \sum_{i=-\infty}^{\infty} b_{j,i}^{(k)} \prod_T (t - iT) \tag{2}$$

$$a_j(t) = \sum_{i=-\infty}^{\infty} a_{j,i} \prod_{T_c} (t - iT_c) \tag{3}$$

where $b_{j,i}^{(k)} \in \{+1, -1\}$ denotes the information bit of $k$th subband of image $j$ in the $i$th time interval, $a_j(t)$ is an infinite random spreading code sequence assigned to the $j$th image with each chip $a_{j,i}$ independent and equiprobably distributed on $+1, -1$, and $\prod_T(\cdot)$ is the unit pulse function of duration $T$, defined by

$$\prod_T(t) = \begin{cases} 1, & t \in [0, T) \\ 0, & \text{else.} \end{cases} \tag{4}$$

The duration of each data bit is $T$, while the duration of each chip in the spreading code signal is $T_c$. As a result, the number of chips per bit is $N = \frac{T}{T_c}$, where $N$ is an integer and usually called the length of the spreading sequence.

The instantaneous optical power of the laser for the $j$th image is

$$P_j(t) = \bar{P}_T \left[ 1 + m \sum_{k=1}^{M} s_{kj}(t) \right] \tag{5}$$

where $\bar{P}_T$ is the driving laser current bias and $m$ denotes the modulation index. For proper optical intensity modulation, $m$ should not be greater than $1/M$ in order to avoid nonlinear operation of the laser, i.e., $1 < m \leq 1/M$. By neglecting the fiber and coupling losses in optical communication channel, the RF photocurrent is identical to the desired signal at each receiver. This would imply that $A = R\bar{P}_T m/N_c$ where $R$ is the responsitivity of the photodiode. The signal energy per bit, $E_b$ is given by

$$E_b = A^2 T/2 = \frac{R^2 \bar{P}_T^2 m^2}{2N_c^2} T. \tag{6}$$

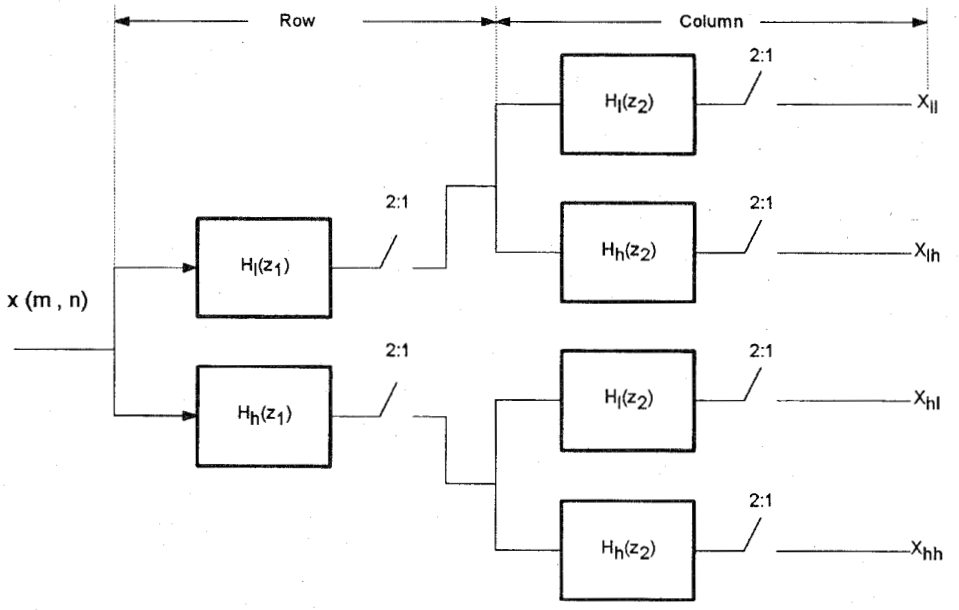


Fig. 3. Separable subband decomposition.

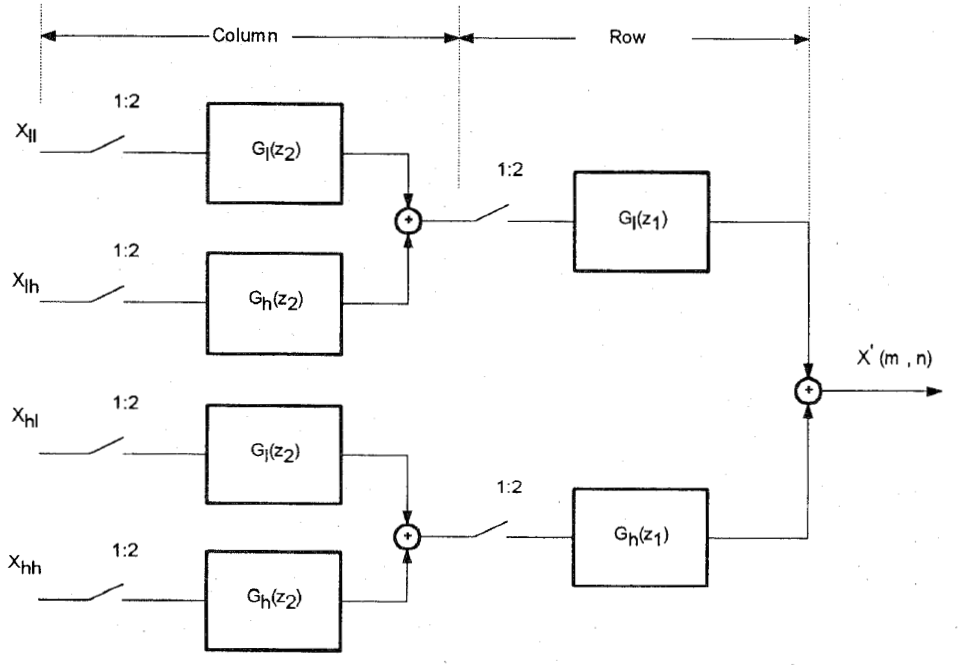


Fig. 4. Separable subband reconstruction.

The maximum achievable values of $A$ and $E_b$ corresponding to $m = 1/M$ and $R = 1$ are

$$A = \bar{P}_T/MN_c = \bar{P}_T/N_s \quad E_b = \frac{\bar{P}_T^2 T}{2M^2 N_c^2} = \frac{\bar{P}_T^2 T}{2N_s^2} \tag{7}$$

where $N_s$ is the total number of subbands (users) which equals $MN_c$.

### B. Receiver Model

Usually, the receiver consists of a silicon avalanche photodiode (APD) detector, $M$ SAW filter-based demodulators, $M$ basedband timing circuits, and $M$ detector circuits. Each SAW device acts as a very high-Q bandpass filter which responds to the signal with a desired subcarrier frequency, and rejects others. After filtering, the SAW matched filter also correlates its input with the preprogrammed matching spreading code sequence and then produces a decision variable used to determine the subband with the matching code.

After performing demodulation, $M$ recovered subbands are upsampled and reassembled by a bank of synthesis filters into a close approximation to the desired image. For simplified analysis, we are interested in the SAW demodulator for the first subband of the first image as the reference demodulator. Hence, the received signal after a high-Q SAW filter with the first subcarrier frequency as its center frequency can be expressed as

$$r(t) = \sum_{j=1}^{N_c} s_j(t-\tau_j) + \sum_{l=1}^{L} s'_l(t-\tau_l) + n(t) \tag{8}$$

where $s_j(t) = s_{1j}(t)$ denotes the first subband of the $j$th image, $s'_l(t)$ is the $l$th harmonics or IMP falling around the center frequency $f_c = f_1$, $L$ is the number of harmonics and IMP's, $n(t)$ is the white Gaussian noise with a double-sided spectral density of $N_0/2$ and $\tau$'s are uniformly distributed over $[0, T]$ because users are independently sending their signals. Moreover, it is shown that $L$ increases with an increase in the number of the subcarriers but the power of each of these harmonics and IMP's decreases by the same factor. Khaleghi and Kavehrad [5] showed that the value of $N_0$ is

$$N_0 = 4KTF/R_L + 2eI_D + (\mathrm{RIN})I_D^2 \tag{9}$$

where $K$ is a Boltzmann's constant ($1.38\times10^{-23} j/\mathrm{K}$), $T$ is an absolute temperature (289 K), $e$ is an electron charge ($1.602 \times 10^{-19}$ C), $F$ is the electronic receiver amplifier noise figure, $R_L$ is the photodiode load resistor, $I_D$ is the total received photocurrent, and the relative intensity noise (RIN) describes noise generated in addition to shot noise by the laser.

Substituting (1) into (8), we have

$$r(t) = A\sum_{j=1}^{N_c} a_j(t-\tau_j)b_j(t-\tau_j)\cos(2\pi f_c t + \theta_j) + A\sum_{l=1}^{L} w_l a'_l(t-\tau_l)\cos(2\pi f_c t + \theta_l) + n(t) \tag{10}$$

where $b_j(t) = b_j^{(1)}(t)$, $\theta_j = -w_c\tau_j + \phi_j$, and $\theta_1$ is assumed to be zero, with no loss in generality. $w_l$ denotes the weight of the $l$th harmonics or IMP. Levels $-40$ dB, $-60$ dB, and $-100$ dB are typical second, third, and a higher order harmonics and IMP's weights, respectively. The amplitude $a'_l(t)$ for the $m$th order IMP or harmonics is proportional to

$$\prod_{i=1}^{m} a_{k_i}(t-\tau_{k_i})b_{k_i}(t-\tau_{k_i}) \tag{11}$$

where $k_i$, $1 \le i \le m$, $\in \{1, 2, \cdots, N_c\}$.

The SAW demodulator is assumed to coherently recover the carrier phase and delay locking to the first subband of image one. This reference demodulator recovers the transmitted data bit by correlating $r(t)$ with the spreading code to construct a decision statistics $Y_i$ for the $i$th data interval, where

$$Y_i = \int_{(i-1)T}^{iT} r(t)a_1(t)\cos(2\pi f_c t)dt. \tag{12}$$

The estimate $\hat{b}_{1,i}$ of the data bit $b_{1,i}$ is determined based on the rule

$$\hat{b}_{1,i} = \begin{cases} 1, & Y_i \ge 0 \\ -1, & Y_i < 0. \end{cases} \tag{13}$$

A bit error occurs if $\hat{b}_{1,i} \ne b_{1,i}$. Note that the procedure of estimating the data bit for all other subbands is identical to that of subband 1.

### C. Average Bit-Error Probability

Substituting (10) into (12) and by the assumption of phase and delay locking to the desired modulated signal, according to the concept of Khaleghi and Kavehrad [5], the output of the reference demodulator, during the $i$th symbol interval, is given by

$$Y_i = \frac{A}{2}b_{1,i} + \frac{A}{2}\sum_{j=2}^{N_c}[b_{j,i-1}R^i_{j,1}(\tau_j) + b_{j,i}\bar{R}^i_{j,1}(\tau_j)]\cos(\theta_j) + \frac{A}{2}\sum_{l=1}^{L} w_l\left(\int_0^T a'_l(t-\tau_l)a_1(t)dt\right)\cos(\theta_l) + \nu \tag{14}$$

where $\nu$ is a Gaussian noise with zero mean and variance $N_0T/4$, $b_{1,i}$ represents the information bit being detected, $b_{j,i-1}$ and $b_{j,i}$ denote the preceding and current bits for the first subband of the $j$th image, respectively. The preceding bit, which, due to the channel delay spread, affects the detection of $b_{1,i}$. In (14), $R^i_{j,1}(\tau_j)$ and $\bar{R}^i_{j,1}(\tau_j)$ are the well known continuous-time partial cross-correlation functions of the regenerated code, $a_1(t)$, and a delayed version of the interfering codes, $a_j(l-\tau_j)$, $2 \le j \le N_c$.

The first term in (14) represents the desired signal to be detected and it has average power $(AT/2)^2 = \bar{P}_T^2T^2/(4N_s^2) = E_bT/2$. The second term in (14) is the inter-image interference which is generated from the first subbands of the other $(N_c-1)$ images. Note that no intra-image subband interferences occur in (14) since a high-Q SAW bandpass filter responds to only the reference subband (i.e., first subband) and rejects the other subbands in the same image. For the simplified derivation of the bit-error probability (BEP), the Gaussian assumption is to take the inter-image interference, harmonics and IMP's as Gaussian noise. Therefore, it can be shown that the interference power is given by

$$P_{\mathrm{int}} = \text{interference power} = (AT/2)^2(N_c-1)\left(\frac{\eta^2}{2}\right) \tag{15}$$

where

$$\eta^2 = E\left\{\frac{\left[b_{j,i-1}R^i_{j,1}(\tau_j) + b_{j,i}\bar{R}^i_{j,i}(\tau_j)\right]^2}{T^2}\right\}. \tag{16}$$

Since $b_{j,i-1}$ and $b_{j,i}$ are independent bipolar variables, the value of $\eta^2$ is found to be approximately equal to $(2/3N)$, where $N$ is the length of spreading code [16]. Thus (15) becomes

$$P_{\mathrm{int}} \approx \frac{\bar{P}_T^2T^2(N_c-1)}{12N_s^2N} = \frac{(N_c-1)T}{6N}E_b = \frac{(N_c-1)}{3N}P_s. \tag{17}$$

Moreover, the total power of the third term of (14) which represents the variance of nonlinear harmonics and IMP's is equal to

$$P_{\text{non}} = \left(\frac{AT}{2}\right)^2 \sum_{l=1}^{L} n_l w_l^2 \eta^2/3 \approx \frac{\bar{P}_T^2 T^2}{18N_s^2 N}\left(\sum_{l=1}^{L} n_l w_l^2\right) = \frac{E_b T}{9N}\left(\sum_{l=1}^{L} n_l w_l^2\right) = P_s\left(\sum_{l=1}^{L} w_l^2(2n_l/9N)\right) \quad (18)$$

where $n_l$ is the order of the $l$th IMP or harmonics and $P_s$ is the received signal power $E_b T/2$.

Observing the above equation, the power suppression of the $n$th order harmonics and IMP's is equal to $(9N/2n)$ when $n_l = n$. Since all the terms in (14) are assumed to be mutually independent, the value of the signal-to-noise plus interference power ratio can be found as

$$\text{SNR} = 2\gamma_b = \frac{P_s}{P_{\text{int}} + P_{\text{non}} + N_0 T/4} = \frac{P_s}{(N_c - 1)(1/3N)P_s + \left(\sum_{l=1}^{L} w_l^2(2n_l/9N)\right)P_s + N_0 T/4} = \frac{E_b}{(N_c - 1)(1/3N)E_b + \sum_{l=1}^{L} n_l w_l^2 (2/9N)E_b + N_0/2} \quad (19)$$

where $\gamma_b$ is the half of the signal-to-noise plus interference power ratio.

If the fiber and coupling losses occur in our system, the received signal power, interference power, and total power of nonlinear harmonics and IMP's would become

$$P_s = \text{received signal power} = \left(\frac{A\alpha_1 T}{2}\right)^2 = \frac{E_b T}{2} \quad (20)$$

$$P_{\text{int}} = \frac{T}{6N}\left(\sum_{j=2}^{N_c} (\alpha_j/\alpha_1)^2\right) E_b = \frac{TE_b}{6N}\left(\sum_{j=2}^{N_c} \xi_j^2\right) \quad (21)$$

$$P_{\text{non}} \approx \left(\frac{A\alpha_1 T}{2}\right)^2 \sum_{l=1}^{L} n_l w_l^2 \eta^2/3 = E_b T/9N\left(\sum_{l=1}^{L} n_l w_l^2\right) \quad (22)$$

where $\xi_j = \alpha_j/\alpha_1$, $1 \le j \le N_c$, $\alpha_j$ is the channel amplitude distortion factor due to the fiber and coupling losses in the transmission of subband 1 from the transmitter of image $j$ to the receiver of image 1, $E_b$ is the received energy per data bit $(E_b = (A\alpha_1)^2 T/2 = \bar{P}_T^2 T\alpha_1^2/(2N_s^2))$. Thus, (19) becomes

$$\text{SNR} = \frac{E_b}{\left(\sum_{j=2}^{N_c} \xi_j^2\right)(1/3N)E_b + \left(\sum_{l=1}^{L} n_l w_l^2\right)(2/9N)E_b + N_0/2}. \quad (23)$$

Ideally, the received signals are intended to be received with equal power. A number of power control mechanisms [17], [18] are trying to compensate for the differing received powers and thus keeping the received powers almost equal. Then $\xi_j = 1$ for $2 \le j \le N_c$ and $\sum_{j=2}^{N_c} \xi_j^2 = N_c - 1$.

Proakis [26] showed that the average BER for binary phase shift keying (BPSK) modulation can be expressed in terms of $\gamma_b$ and is given by

$$p_e = p(\gamma_b) = \frac{1}{2}\text{erfc}(\sqrt{\gamma_b}). \quad (24)$$

## III. Low-Complexity Subband Coding Using Separable Symmetric Short-Kernel Filter Banks

Woods and O'Neil [7] treated 2-D subband analysis/synthesis using both separable and nonseparable filter banks. The most computationally efficient approach to splitting and merging subband images results from using separable filters. The separable subband decomposition is performed in two stages using 1-D filters that process the data along the rows and columns of the image data array (Figs. 3 and 4). The input signal $x$ is first applied to horizontal filters $H_l(z_1)$ (lowpass) and $H_h(z_1)$ (highpass), and horizontally downsampled to get the signals $x_l$ and $x_h$, respectively. In the second stage of the decomposition, each of the signals $x_l$ and $x_h$ is applied to the two vertical filters $H_l(z_2)$ (lowpass) and $H_h(z_2)$ (highpass), and vertically downsampled to get the subband signals $x_{ll}$, $x_{lh}$, $x_{hl}$, and $x_{hh}$. For the purpose of reconstruction, the signals are merges and by upsampling and filtering using the symthesis filters. The vertical synthesis filters are denoted by $G_l(z_2)$ (lowpass) and $G_h(z_2)$ (highpass), and the horizontal synthesis filters are denoted by $G_l(z_1)$ (lowpasss) and $G_h(z1)$ (highpass).

According the separability characteristics of $H_{xy}(z_1, z_2)$ and $G_{xy}(z_1, z_2)$, the 2-D filtering can be implemented as a product of 1-D filtering operations [15]

$$H_{xy}(z_1, z_2) = H_x(z_1)H_y(z_2) \quad (25)$$

$$G_{xy}(z_1, z_2) = G_x(z_1)G_y(z_2) \quad (26)$$

where $x$ and $y$ denote $l$ (lowpass) or $h$ (highpass).

Moreover, it is shown that the 2-D exact reconstruction filters for $H_{xy}(z_1, z_2)$ and $G_{xy}(z_1, z_2)$ can be developed in terms of 1-D exact reconstruction filters. In designing 1-D exact reconstruction filters, we should focus on an analysis into a two-channel system. The analysis filter bank splits the input signal into two-channel signals by processing it with a lowpass filter $H_l(z)$ in one path and with a highpass filter $H_h(z)$ in the other. The filtered signals $u_0$ and $u_1$ are downsampled by a factor of two to obtain the subband signals $x_l$ and $x_h$. In a back-to-back connection, these signals are upsampled and processed by the synthesis filters with transfer functions $G_l(z)$ and $G_h(z)$. In other words, every second sample has been discarded by the downsampling and has been reinserted as a zero-valued sample by the upsampling. The aliasing distortion in the reconstruction can be removed if the synthesis filters are defined as

$$\begin{cases} G_l(z) = H_h(-z) \\ G_h(z) = -H_l(-z). \end{cases} \quad (27)$$

Quadrature mirror filters (QMF's) [13] have been proposed and widely used as analysis and synthesis filters in subband coding of images. However, Irie and Kishimoto [10] showed that QMF's do not permit reconstruction to be exact, although

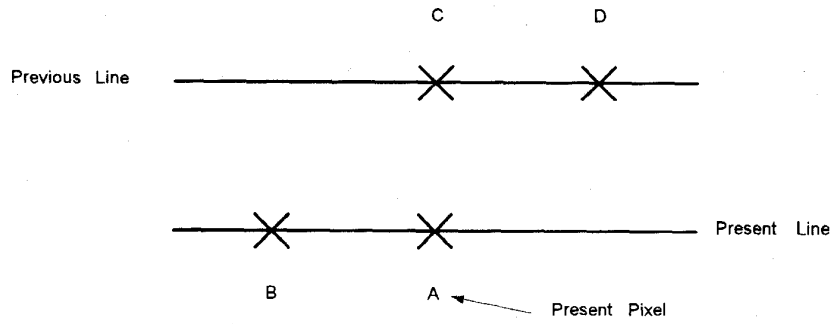


Fig. 5. Configuration of pixels used for prediction.

the reconstruction error can be made very small by using long tap filters. For video and digital image applications, use of such long tap filters, while not providing any significantcoding gain, may increase the hardware complexity. Since the processing of video signals in wireless channels involves high sampling rates, it is very desirable to keep the filter bank complexity low. Symmetric short-kernel filters (SSKF's) have been considered as the low complexity subband decomposition and reconstruction filter pairs because of the simplicity in implementation [9]. The SSKF's are the symmetric short filters which are obtained by factoring a product filter, $P(z) = H_l(z)H_h(-z)$ into linear phase components. Le Gall *et al.* [9] showed that an example of the lowpass and highpass analysis filters with the simplest coefficients is given by

$$\begin{cases} H_l(z) = \left(\frac{1}{2} + \frac{1}{2}z^{-1}\right) \\ H_h(z) = \left(\frac{1}{2} - \frac{1}{2}z^{-1}\right). \end{cases} \tag{28}$$

Similarly, from (27) and (28), the synthesis filters are

$$\begin{cases} G_l(z) = H_h(-z) = \left(\frac{1}{2} + \frac{1}{2}z^{-1}\right) \\ G_h(z) = -H_l(-z) = -\left(\frac{1}{2} - \frac{1}{2}z^{-1}\right). \end{cases} \tag{29}$$

The two-tap filters of (28)–(29) are implementable using a small number of shift and add operations. The use of general multipliers is avoided. This leads to a simple and computationally efficient subband coding implementation. Note that the decomposition of the input image can be extended to more than four bands by repeating the separability process to each subband image in a tree-structured manner.

### A. Coding of Subband Signals

To achieve maximum compression with high image fidelity, the subbands have to be encoded on a perceptual basis by following proper coding strategy. The subband signal carrying the lowest frequency information usually has a high degree of spatial correlation that is suitable for coding using either predictive techniques such as differential pulse code modulation (DPCM) or transform coding using discrete cosine transform [8], [15]. Since the baseband contains the most information, so this band is quantized as accurately as possible. The high frequency subbands contain edge and contour information. These subband signals can be directly quantized by coarse quantizers since the noise produced by quantizing higher bands with a few levels can easily be tolerated by the human eye, and then PCM encoded in the spatial domain. A large fraction of the quantized data in the high frequency band signals consists of zero samples and these signals are, therefore, well suited for runlength encoding [8].

The baseband has a histogram that is similar to the original image with high pixel-to-pixel correlation. Due to this high correlation, DPCM encoder is chosen to code the subband. The pixel configuration for the two-dimensional prediction is shown in Fig. 5. The predicted value is given by

$$\hat{x}_A = bx_B + cx_C + dx_D \tag{30}$$

where $x_B$, $x_C$, and $x_D$ are previously reconstructed pixels, and $\hat{x}_A$ is the prediction of the present pixel. The weighting factors, $b$, $c$, and $d$ are chosen to be 0.5, 0.25, and 0.25, respectively. The prediction error signal is then quantized by a symmetric nonuniform quantizer. Variable-length code (Huffman) is used to encode the quantized prediction error signal of the baseband.

An optimal approach in the minimum mean square sense is to design a quantizer which matches the probability density function of the input signals (close to a generalized Gaussian or Laplacian probability density function, pdf). This optimal quantizer is known as Lloyd–Max quantizer. However, Gharavi and Tabatabai [8] showed that such a quantizer is not suitable for encoding the higher frequency band signals. This is mainly due to the existence of picture noise which manifests itself as a low level signal within these bands, and would result in a fine quantization of the noise. To circumvent this problem, they proposed a highly efficient nonuniform symmetric quantizer with center dead zone to quantize the high bands. The dead zone is used to eliminate the picture noise. The input values in the active region are then uniformly quantized to $L$ levels. Usually, Huffman codes are used to encode the quantized nonzero pixel values. Meanwhile, the quantized high bands are observed to have a large number of connected areas of zeros. Therefore, run-length coding techniques are implemented as 1-D codes for this purpose.

When aiming for a constant bit rate for each subband via the hybrid CDMA/SCM system, it is convenient to assume that each subband is encoded into a constant number of bits and its output rate is monitored on a line-by-line basis. The instantaneous bit rate of the specific line being encoded is compared against its targeted rate, and its dead zone is appropriately increased, decreased, or maintained. In addition, a buffer is used to smooth out the variations in the rate. Then

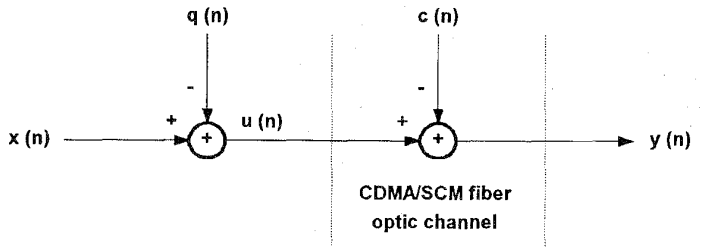


Fig. 6. Transmission of quantized amplitudes over CDMA/SCM fiber-optic channels, where $q(n)$ and $c(n)$ denote quantization error and the sum of total CDMA interference, SCM's IMP, and AWGN noise, respectively.

the bit rate is kept constant for each subband. More details about the bit rate control can be found in [15].

## IV. Image Quality Evaluation for CDMA/SCM Subband Image Transmission

In this section, we would like to introduce an analysis of channel error effects in the subband image transmission via a fiber-optic CDMA/SCM channel. This would provide an useful tool to evaluate the quality of subband image transmission over the CDMA/SCM channel. The image quality can be characterized by a closed expression which is a logarithmic function in terms of transmission error variances for those subbands. Fortunately, this useful expression can be obtained by the similar procedure proposed by our companion papers [30], [31]. As discussed in Section III, there are two encoding techniques for subband images. The baseband is encoded using DPCM, and higher bands are PCM encoded. Fig. 6 shows that the reconstructed output signal $y(n)$ includes the effects of both quantization error, $q(n)$ and channel error due to the sum of CDMA interference, SCM's, IMP, harmonics noise, and thermal noise, $c(n)$.

### *A. Transmission Errors in Both PCM and DPCM Codings via Fiber-Optic CDMA/SCM Channels*

The total reconstruction error variance for the PCM encoding is defined by

$$\sigma^2_{r,\mathrm{PCM}} \equiv E\{(x-y)^2\} \tag{31}$$

where $x$ is the input signal and $y$ is the reconstructed output signal.

Jayant and Noll [21] showed that $\sigma^2_{r,\mathrm{PCM}}$ of (31) can be written as

$$\sigma^2_{r,\mathrm{PCM}} = \sigma^2_{q,\mathrm{PCM}} + \sigma^2_{m,\mathrm{PCM}} + \sigma^2_c \approx \sigma^2_{q,\mathrm{PCM}} + \sigma^2_c \tag{32}$$

where $\sigma^2_{q,\mathrm{PCM}}$ and $\sigma^2_c$ are quantization error variance and channel error variance, respectively. Note that the crosscorrelation, $\sigma^2_{m,\mathrm{PCM}}$ between quantization and channel errors is nearly equal to zero if the quantizer characteristics are close to that of an optimal quantizer [20], [28]. For simplicity, we assume the transmission errors occur randomly in the received sequence, and each error affects the transmitted symbol independently. Furthermore, the transmission errors are assumed to be Gaussian distributed. This channel is called the memoryless random-error additive white Gaussian noise (AWGN) channel. Under the above assumptions, Noll [20] and R. Steele *et al.* [28] found that the channel error variance $\sigma^2_c$ can be expressed in terms of the BEP, $p_e$, and is given by

$$\sigma^2_c = \epsilon^2_c \cdot \sigma^2_x \tag{33}$$

and

$$\epsilon^2_c = \sum_{j=1}^{R} \xi_j {p_e}^j \tag{34}$$

where $\epsilon^2_c$ is called the channel performance factor, and $R$ is the number of bits used to represent the quantizer output and $\xi_j$ are channel coefficients that reflect the effects on $\sigma^2_c$ of the quantizer characteristics, the chosen binary code and the source statistics. For example, $\xi_1 = 2.55$, $\xi_2 = 4.97$, $\xi_3 = 6.91$ when natural binary code is chosen and a nonuniform quantizer is used. However, Noll's expression of (33) and (34) may fail when the CDMA/SCM fiber-optic channels are modeled as the burst-error channels with memory. Bursty bit errors are much more difficult to correct than random bit errors. Fortunately, the bursty errors can be randomized by a process of interleaving so that the error pattern appearing in the interleaved data stream will resemble that of random bit errors. Steele *et al.* [28] showed that the expression of channel error variance in PCM transmission over burst-error channels is quite similar to that of (33) and (34) when the PCM bit stream is interleaved (or scrambled) prior to its transmission.

Combining (32) and (33), it yields

$$\sigma^2_{r,\mathrm{PCM}} = \left(\epsilon^2_{q,\mathrm{PCM}} + \epsilon^2_c\right)\sigma^2_x \tag{35}$$

where $\epsilon^2_{q,\mathrm{PCM}}$ is the PCM quantizer performance factor.

Jayant and Noll [21] also showed that the total reconstruction error variance for DPCM in the presence of random channel errors can be expressed as the sum of three separate components

$$\sigma^2_{r,\mathrm{DPCM}} = \sigma^2_{q,\mathrm{DPCM}} + \sigma^2_{m,\mathrm{DPCM}} + \gamma\sigma^2_c \tag{36}$$

$$\gamma = \sum_{k=0}^{\infty} h^2_{\mathrm{DEC}}(k) = \frac{1}{2\pi}\int_{-\pi}^{\pi} |H_{\mathrm{DEC}}(w)|^2 dw \tag{37}$$

where $\gamma$ is called the power transfer factor, $h_{\mathrm{DEC}}(n)$ is the impulse response of the discrete decoder filter of the DPCM, and $H_{\mathrm{DEC}}(w)$ is its transfer function. Moreover, the quantity $\sigma^2_{m,\mathrm{DPCM}}$ has been found to be negligible compared to both $\sigma^2_{q,\mathrm{DPCM}}$ and $\sigma^2_{c,\mathrm{DPCM}}$ [21], [29]. Thus $\sigma^2_{r,\mathrm{DPCM}}$ of (36) reduces to

$$\sigma^2_{r,\mathrm{DPCM}} \approx \left(\epsilon^2_{q,\mathrm{DPCM}} + \gamma\epsilon^2_c\right) G_p^{-1}\sigma^2_x \tag{38}$$

where $\epsilon^2_{q,\mathrm{DPCM}}$ is the DPCM quantizer performance factor and $G_p$ is the prediction gain which is defined as the ratio between the input signal variance and the prediction error variance. In addition, Modestino and Daut [29] proposed an alternative formulation which is quite similar to Jayant and Noll's expression of (38). Comparing (38) with (35), it may be found that the quantization noise contribution in DPCM is smaller than in PCM by a factor $G_p$; and the channel error contribution in DPCM is smaller than in PCM by a factor $\frac{G_p}{\gamma}$, provided that $\epsilon^2_{q,\mathrm{DPCM}}$ is equal to $\epsilon^2_{q,\mathrm{PCM}}$. Note that the ratio between $\epsilon^2_{q,\mathrm{PCM}}$ and $\epsilon^2_{q,\mathrm{DPCM}}$ is equal to unity for generalized Gaussian images or $\frac{2}{9}$ for Laplacian images [21].

### *B. Analysis of Channel Errors in Subband Image Transmission over Fiber-Optic CDMA/SCM Channels*

From the above discussion, $\sigma^2_{r,\mathrm{DPCM}}$ is regarded as the reconstruction error variance for base band, $\sigma^2_{s1}$, and $\sigma^2_{r,\mathrm{PCM}}$'s are used to characterize the reconstruction error variances for higher bands, $\sigma^2_{sk}, k > 1$. Moreover, [22], [23] showed that the reconstruction error variance of an image via $M$ parallel independent virtual channels can be obtained by performing a weighted sum of total subband reconstruction error variances, i.e.,

$$\sigma^2_{\mathrm{image}} = \sum_{k=1}^{M} \beta_k \sigma^2_{sk} \tag{39}$$

where the weighting value for the $k$th subband is specified by

$$\beta_k = \frac{1}{(2\pi)^2} \int_{-\pi}^{\pi} \int_{-\pi}^{\pi} |G_k(w_1, w_2)|^2 dw_1 dw_2 \tag{40}$$

where $G_k(w_1, w_2)$ is the transfer function of the synthesis filter for the $k$th subband. However, for the case of separable reconstruction filters and $M = 4$, the weighting values are $\beta_{ll} = \beta_l^2$, $\beta_{lh} = \beta_{hl} = \beta_h \beta_l$ and $\beta_{hh} = \beta_h^2$, where $\beta_l$ and $\beta_h$ are given by

$$\begin{aligned} \beta_l &= \frac{1}{2\pi} \int_{-\pi}^{\pi} |G_l(w)|^2 dw \\ \beta_h &= \frac{1}{2\pi} \int_{-\pi}^{\pi} |G_h(w)|^2 dw. \end{aligned} \tag{41}$$

Cheong *et al.* [21] found that both QMF and orthonormal wavelet have a value nearly equal to unity ($\beta_l = \beta_h \approx 0.9999$), and SSKF has low values ($\beta_l = 0.75$ and $\beta_h = 0.359\,375$). This implies that SSKF achieves much smaller image reconstruction error variance than both QMF and orthonormal wavelet. In (39), each of the $M$ parallel virtual channels corresponds to the subcarrier-code pair of a particular subband in the reference image. $\sigma^2_{sk}$ represents the error variance of the $k$th received subband in this reference image via both the $k$th subcarrier and the spreading code corresponding to the image.

Recently, Irie and Kishimoto [10] and Lu *et al.* [24] proposed a modified symmetric short-kernel filters which can achieve the quantization-error-free reconstruction for the subband images by using both PCM and DPCM codings. The modified SSKF's involve performing two kinds of transformations on the original two-tap SSKF's of (28), i.e., transformation by criterion decision and transformation by integer/noninteger decision. Moreover, they showed that the quantization errors can be totally eliminated when more than ten bits, $R \geq 10$, are used to represent the quantization levels of PCM and DPCM codings for the subbands based on the modified SSKF's. In summary, the quantizer performance factors, $\epsilon^2_q$'s of (35) and (38) vanish when the modified SSKF's with more than ten quantization bits are used. Therefore, from (33), (35), (38), and (39), it yields

$$\sigma^2_{\mathrm{image}} = \left( \beta_1 \gamma \epsilon^2_{c1} G_p^{-1} + \sum_{k=2}^{M} \beta_k \epsilon^2_{ck} \right) \sigma^2_x. \tag{42}$$

From (42), the signal-to-noise ratio (SNR) of the output image [21] becomes

$$\begin{aligned} \mathrm{SNR}_{\mathrm{image}} &= 10 \log_{10} \frac{Ex^2}{E(x-y)^2} \quad \text{(dB)} \\ &= -10 \log_{10} \left( \beta_1 \gamma \epsilon^2_{c1} G_p^{-1} + \sum_{k=2}^{M} \beta_k \epsilon^2_{ck} \right) \end{aligned} \tag{43}$$

where $x$ and $y$ denotes the input and output gray values.

It should be mentioned that the BEP's of the subbands in the same image are identical since each of them has the same inter-image subband interferences and noise over the fiber-optic channel. If $p_e$ and $R$ are sufficiently small, the channel contributes to $\epsilon^2_c$ only through single errors. Thus, $\epsilon^2_{ck} \approx \xi^k_1 p_e$ for the $k$th subband, and $\mathrm{SNR}_{\mathrm{image}}$ of (43) becomes

$$\mathrm{SNR}_{\mathrm{image}} \approx C - 10 \log_{10} p_e \tag{44}$$

where $\xi^k_1$ is the first channel coefficient of (34) for the $k$th subband in the reference image, and $C = -10 \log_{10} (\beta_1 \gamma \xi^1_1 G_p^{-1} + \sum_{k=2}^{M} \beta_k \xi^k_1)$ would be a constant which is independent of BEP. In other words, $C$ does not depend on the total interference and noise over CDMA/SCM fiber-optic channels. However, the commonly-used subjective measure of the reconstructed image quality is the peak signal-to-noise ratio (PSNR) [21] defined by

$$\begin{aligned} \mathrm{PSNR} &= 10 \log_{10} \frac{x^2_{pp}}{E(x-y)^2} \quad \text{(dB)} \\ &\approx \tilde{C} - 10 \log_{10} p_e \quad \text{(dB) for } p_e \\ &\qquad \text{and } R \text{ are sufficiently small} \end{aligned} \tag{45}$$

where $x_{pp}$ is the peak gray value of the input image, $\tilde{C} = C + 10 \log_{10} \frac{x^2_{pp}}{\sigma^2_x}$ is also independent of the total interference nonlinear IMP's and harmonics, and thermal noise over CDMA/SCM fiber-optic channels. Both (43) and (45) show that PSNR is increasing while $p_e$ is decreasing since $\epsilon_{ck} = f_k(p_e)$ is a monotonically increasing function of bit error probability. However, the relationship between PSNR and $p_e$ is quite complicated and cannot be characterized by a function of simple expression. When $p_e$ becomes sufficiently small, from (45), PSNR is inversely related to a simple logarithmic function of $p_e$.

## V. Simulation Results

To evaluate the performance of the transmission of subband images via CDMA/SCM fiber-optic channels, two mono-

Fig. 7. Test image "Girl."

Fig. 8. Test image "London."

(a)

(b)

Fig. 9. (a) The reconstructed "Girl" image via CDMA/SCM fiber-optic channels when $\frac{E_b}{N_0} = 9$ dB. (b) The reconstructed "London" image via CDMA/SCM fiber-optic channels when $\frac{E_b}{N_0} = 9$ dB.

chrome test images, "Girl" illustrated in Fig. 7 and "London" illustrated in Fig. 8 are considered in our system. They are gray scale pictures with 256 $\times$ 256 pixels and 8 b per pixel. For each picture, the input was first split into four bands using a modified two-dimensional separable SSKF (two-tap in each direction) proposed by Irie *et al.* [10], [25]. The lowest band image was DPCM encoded using 2-D prediction and a nonuniform quantizer with ten quantization bits and subsequent variable length coding. However, since the samples in the higher frequency bands show little correlation among pixels, these bands are encoded using PCM with the nine-bit nonuniform quantizer instead of DPCM. More recently, Irie *et al.* [10], [25] and Lu *et al.* [24] showed that this nine-bit nonuniform quantizer for PCM coding is able to achieve an acceptable small quantization error as well as 10-b quantizer.

Next, we consider the transmission of these test pictures over a hybrid CDMA/SCM fiber-optic channels with two spreading codes ($N_c = 2$) and four subcarriers ($M = 4$) which correspond to these two pictures and their four subbands respectively. The spreading codes are Gold codes of periodic length 127, e.g., $N = 127$. The Gold sequences are obtained by multiplying two primitive polynomials $x^7 + x^3 + x^2 + x + 1$ and $x^7 + x^3 + 1$ [18]. From (18), the power suppression of second order harmonics and IMP's in the light source nonlinearity is equal to $9N/4$ ($=285.75$) and the third order IMP's and harmonics are suppressed by the factor $9N/6$ ($=190.5$) and in general the $n$th order components are suppressed by a factor $9N/2n$ ($=571.5/n$). Assume that each subband is transmitted with a bit rate of 80 kb/s, using a chip rate of 10 Mchips/s. This means that 20 MHz double-sided subcarrier modulation band can be reused by the subcarrier, as long as they are 80 kHz apart. Therefore, the four subcarrier frequencies are chosen to be 120 MHz, 120.08 MHz, 120.16 MHz, and 120.24 MHz, respectively.

Moreover, the CDMA/SCM fiber-optic channel output is corrupted a zero-mean AWGN with a double-sided spectral density, $\frac{1}{2}N_0$ defined in (9). Fig. 9 shows the reconstructed pictures of both "Girl" and "London" when the channel SNR of each subband, $E_b/N_0$, is assumed to be 9 dB. In Fig. 10,

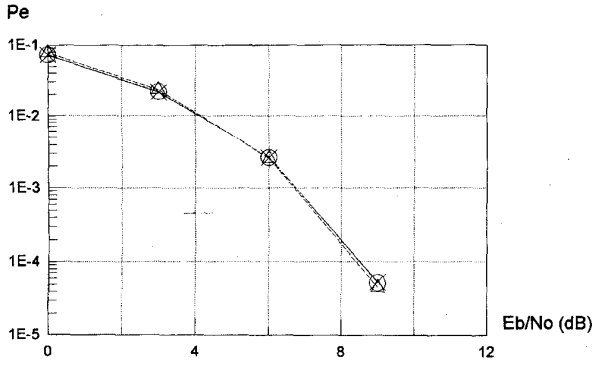


Fig. 10. The BER's of both the "Girl" and "London" images via CDMA/SCM fiber-optic channels. (△: theoretic BER, o: Girl image, ×: London image.)

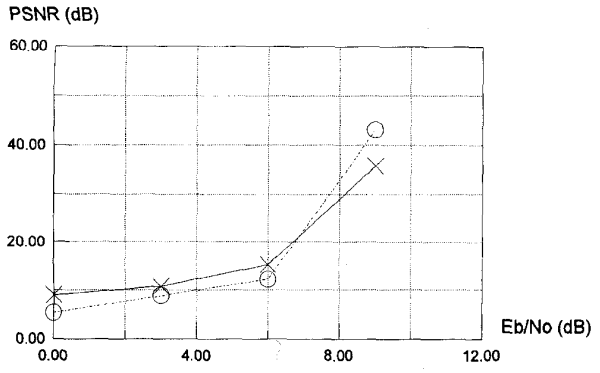


Fig. 11. PSNR performances versus channel SNR for both the "Girl" and "London" images via CDMA/SCM optic-fiber channels. (o: Girl image, ×: London image.)

the BEP's of both test images are plotted versus the channel SNR of their reference first subbands. It is clearly from this figure that the average BEP's for both test images are close to a desired theoretic BEP of $p_e = p(\gamma_b(E_b/N_0)) = f(E_b/N_0)$ shown in (24), where $\gamma_b$ defined in (19) can be expressed as a function of $E_b/N_0$. Fig. 11 illustrates the image peak SNR versus channel SNR, $E_b/N_0$, performances of both test images via CDMA/SCM systems. These two PSNR curves are almost identical since the received powers of all the subbands are identical. In Fig. 11, the PSNR curve for "Girl" or "London" is inversely related to its BER curve shown in Fig. 10. However, PSNR is a complicated monotonically decreasing function of $p_e$ when the channel SNR value falls within an interval between 3 dB and 6 dB. The quality of image transmission via CDMA/SCM system rapidly deteriorates with the image SNR becoming an unreliable quality measure when the channel SNR is lower than 5 dB. It may be observed from Fig. 11 that the two reconstructed pictures via CDMA/SCM systems attain almost identical image PSNR of 35 dB at channel SNR of 9 dB. The PSNR of 35 dB is a practical performance index which allows error-free image transmission [21].

## VI. Conclusion

An image transmission system over CDMA/SCM fiber-optic channels is investigated in this paper. The adoption of subband coding techniques using SSKF's which require very few computations to divide the image information into a number of subbands, instead of transmitting the image over the fiber-optic channel directly, enables fully parallel subband image transmission and access. Each subband is transmitted using a unique subcarrier-code pair, and fits within the narrow-band data rate requirement in SCM systems. After transmission, each received signal can be detected by a high-Q SAW demodulator with the matching subcarrier-code pair. These recovered subbands are reassembled into a close approximation to the input image. We also introduced an analysis of transmission error effects in the subband image via CDMA/SCM fiber-optic channels. Finally, simulation results for two commonly-used test images were presented and compared with the analysis.

## References

[1] "Special issue on applications of RF microwave subcarriers to optical fiber transmission in broadband networks," *IEEE J. Select. Areas Commun.*, vol. 8, Sept. 1990.
[2] CCITT Recommendation H.261, Video Codec for Audiovisual Services at $p \times 64$ kbit/s, Dec. 1990.
[3] R. M. Gagliardi, A. J. Mendez, M. R. Dale, and Z. Park, "Fiber-optic digital video multiplexing using optical CDMA," *J. Lightwave Technol.*, vol. 11, no. 1, pp. 20–26, Jan. 1993.
[4] K. I. Kitayama, "Novel spatial spread spectrum based fiber optic CDMA networks for image transmission," *IEEE J. Select. Areas Commun.*, vol. 12, no. 4, pp. 762–772, May 1994.
[5] F. Khaleghi and M. Kavehrad, "A subcarrier multiplexed CDM optical local area network, theory and experiment," *IEEE Trans. Commun.*, vol. 43, no. 1, pp. 75–87, Jan. 1995.
[6] M. Kavehrad, F. Khaleghi, and G. Bodeep, "An experiment on a CDM subcarrier multiplexed optical-fiber local area network," *IEEE Photon. Technol. Lett.*, vol. 4, no. 7, pp. 793–796, July, 1992.
[7] J. W. Woods and S. D. O'Neil, "Subband coding of images," *IEEE Trans. Acoust., Speech, Signal Processing*, vol. ASSP-34, pp. 1278–1288, Oct. 1986.
[8] H. Gharavi and A. Tabatabai, "Subband coding of monochrome and color images," *IEEE Trans. Circuits Syst.*, vol. CAS-35, no. 2, pp. 207–214, Feb. 1988.
[9] D. Le Gall and A. Tabatabai, "Subband coding of digital images using symmetric short kernel filters and arithmetic coding technique," in *IEEE Proc. ICASSP*, New York, Apr. 1988, pp. 761–764.
[10] K. Irie and R. Kishimoto, "A study on perfect reconstruction subband coding," *IEEE Trans. Circuits Syst. Video Technol.*, vol. 1, no. 1, pp. 42–48, Mar. 1991.
[11] G. Karlsson and M. Vetterli, "Three dimensional subband coding of video," in *IEEE Proc. ICASSP*, Apr. 1988, pp. 1100–1103.
[12] M. Vetterli, "Multi-dimensional subband coding: Some theory and algorithms," *Signal Processing*, vol. 6, pp. 97–112, Apr. 1984.
[13] H. Gharavi and A. Tabatabai, "Subband coding of digital images using two-dimensional quadrature mirror filtering," in *Proc. SPIE Vis. Commun. Image Process.*, Cambridge, MA, Sept. 1986, pp. 51–61.
[14] M. J. T. Smith and T. P. Barnwell III, "Exact reconstruction techniques for tree structured subband coders," *IEEE Trans Acoust., Speech, Signal Processing*, vol. ASSP-34, pp. 434–441, June 1986.
[15] H. Gharavi, "Subband coding of video signals," in *Subband Image Coding*, J. W. Woods, Ed. Norwell, MA: Kluwer, 1991.
[16] M. B. Pursley, "Spread spectrum multiple access communications," in *Multi-User Communication Systems*. New York: Springer-Verlag, 1981, pp. 139–199.
[17] K. S. Gilhousen *et al.*, "On the capacity of a cellular CDMA system," *IEEE Trans. Veh. Technol.*, vol. 40, no. 5, pp. 303–312, 1991.
[18] W. C. Y. Lee, "Power control in CDMA," in *Proc. VTC*, 1991, pp. 77–80.
[19] G. L. Turin, "The effects of multipath and fading on the performance of direct-sequence CDMA systems," *IEEE J. Select. Areas in Commun.*, vol. SAC-2, no. 4, pp. 597–603, July, 1984.
[20] P. Noll, "Effects of channel errors on the signal-to-noise performance of speech-encoding systems," *Bell System Tech. J.*, pp. 1615–1636, Nov. 1975.
[21] N. S. Jayant and P. Noll, *Digital Coding of Waveforms*. Englewood Cliff, NJ: Prentice-Hall, 1984.

[22] C. K. Cheong, K. Aizawa, T. Saito, and M. Hatori, "Subband image coding with biorthogonal wavelets," *IEICE Trans. Fundamentals*, vol. E75-A, no. 7, pp. 871–880, July, 1992.
[23] J. Katto and Y. Yasuda, "Performance evaluation of subband coding and optimization of its filter coefficients," in *Proc. SPIE Visual Commun. Image Processing*, Boston, MA, Nov. 1991, pp. 95–106.
[24] Ç. C. Lu, N. Omar, and Y. Q. Zhang, "A modified short-kernel filter pair for perfect reconstruction of HDTV signals," *IEEE Trans. Circuits Syst. Video Technol.*, vol. 3, no. 2, pp. 162–164, Apr. 1993.
[25] K. Irie, Y. Okumura, N. Sakurai, and R. Kishimoto, "High-quality subband Codec for HDTV transmission," *IEEE Trans. Circuits Syst. Video Technol.*, vol. 4, no. 4, pp. 195–200, Apr. 1995.
[26] J. G. Proakis, *Digital Communication*, 2nd edn. New York: McGraw-Hill, 1989.
[27] G. Vannucci, "Combining frequency-division and code-division multiplexing in a high-capacity optical network," *IEEE Network*, pp. 21–30, Mar. 1989.
[28] R. Steele, C. E. Sunberg, and W. C. Wong, "Transmission errors in companded PCM over Gaussian and Rayleigh fading channels," *AT&T Bell Lab. Tech. J.*, vol. 63, no. 6, pp. 955–990, July-Aug. 1984.
[29] J. W. Modestino and D. Daut, "Combined source-channel coding of images," *IEEE Trans. Commun.*, vol. COM-27, no. 11, pp. 1644–1659, Nov. 1979.
[30] B. C. Wang and P. R. Chang, "Spread spectrum multiple-access with DPSK modulation and diversity for image transmission over indoor radio multipath fading channels," *IEEE Trans. Circuits Syst. Video Technol.*, vol. 6, no. 2, pp. 200–214, Apr. 1996.
[31] P. R. Chang, "Spread spectrum CDMA systems for subband image transmission," *IEEE Trans. Veh. Technol.*, to appear.

**Po-Rong Chang** (M'87), for a photograph and biography, see this issue, p. 1830.

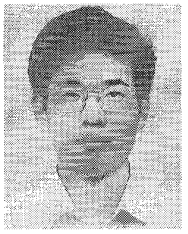

**Chih-Chiang Chang** was born on December 28, 1967, in Hsin-Chu, Taiwan, ROC. He received the B.S. and M.S. degrees from the National Chen-Kung University, Tainan, Taiwan, ROC, both in electrical engineering, in 1990 and 1992, respectively.

He is presently working toward the Ph.D. degree in Communication Engineering at the National Chiao-Tung University, Hsin-Chu, Taiwan, ROC. His current research interests are in wireless multimedia system, CDMA cellular system, color image processing, and fuzzy neural network.